AIAA 80-0155R

Numerical Design and Analysis of Optimal Slot Shapes for Transonic Test Sections—Axisymmetric Flows

K. R. Karlsson* and Y. C.-J. Sedin†
Saab-Scania AB, Linköping, Sweden

A method for calculating transonic wind-tunnel wall interference in axisymmetric slotted test sections is studied. The problem of designing slot shapes for minimum interference is also addressed. The considered slot flow model is inviscid. On finding the wall interference, a filtered small disturbance velocity potential is iteratively solved between the wall and the body, repeatedly using a homogeneous wall boundary condition. When designing an optimal slot for a given body the desired free airflow at the wall is the main input. Thus, there is no need for repeated field calculations within the test section to create a slot. A number of cases for nonoptimal and optimal slots are shown at design and off-design conditions for three axisymmetric bodies.

Nomenclature

$A(x)$ = $\ln(a(x))$, logarithm of slot width, Eq. (6)
$a(x)$ = slot width, Fig. 4
B = blockage ratio of test section, %, Table 1
C_p = $(p-p_\infty)/(\rho_\infty U_\infty^2/2)$, pressure coefficient
E = unit step function; $E(y)=1, y\geq 0$; $E(y)=0, y<0$
$\mathfrak{F}$ = wall boundary condition functional, Eq. (1)
F = $r\tilde{\varphi}_r$, Eq. 3
FTI = figure of tunnel interference, Eq. (8)
G = $\tilde{\varphi}-\ln(r)F$, Eq. (3)
l = slot depth, Fig. 4
L = full body length, Fig. 3
m = parameter of generalized parabolic arc body, Eq. (14)
M_∞ = Mach number of freestream reference flow
M_0 = test section entrance Mach number (approx $M_0=M_\infty\sqrt{1-(\gamma+1)\delta}$), Fig. 2
N = number of slots
p = pressure
p_p = pressure in plenum chamber
p_∞ = pressure in freestream reference flow
q = slot volume flux/unit length, Eq. (4)
Q = normalized slot flow potential, Eqs. (6) and (10)
R = radius of body, Eq. (14)
r = radius vector in crossflow plane ($r=1$ at tunnel wall)
U_∞ = velocity in freestream reference flow
v = normalized slot flow velocity at y_p, Eq. (11)
x = distance along tunnel axis
x_0 = slot start, upstream boundary of computational domain
x_D = distance along body from nose tip to maximum diameter, Fig. 3
y, z = Cartesian coordinates at slot, Figs. 1 and 4
y_p = coordinate of line in slot centerplane where the plenum pressure is imposed, Figs. 1 and 4
y_{p0} = y_p in the "jet region," Fig. 1
γ = specific heat ratio ($\gamma=1.4$)
δ = $(p_p-p_\infty)/(\rho_\infty U_\infty^2)$ normalized plenum pressure
δ^* = boundary-layer displacement thickness at wall
φ = perturbation velocity potential to "exact" problem
$\tilde{\varphi}$ = perturbation velocity potential to approximate (filtered) problem, Eq. (2)
$\tilde{\varphi}_0$ = integration constant given at beginning of slot, Eq. (6)
ρ_∞ = density of freestream reference flow
τ = slenderness ratio, Eq. (14)

Presented as Paper 80-0155 at the AIAA 18th Aerospace Sciences Meeting, Pasadena, Calif., Jan. 14-16, 1980; submitted Jan. 16, 1980; revision received July 1, 1980.

*Research Engineer, Systems Development Laboratory, Aerospace Division.

†Senior Research Engineer, Department of Aerodynamics, Aerospace Division. Member AIAA.

I. Introduction

WIND-TUNNEL wall interference constitutes a serious problem when testing models in the transonic speed regime. A simple and practically proved way to diminish the level of interference is to ventilate the tunnel walls through a limited number of longitudinal slots. Other ideas such as porous or solid adaptive walls are of course also possible solutions, although the latter seem to be rather complicated to realize in practice. As there already exists a number of old wind-tunnel facilities with slotted test sections, it would perhaps be worthwhile to rebuild some of these to improve on the flow quality and to minimize the wall interference further. To that end a computational method is urgently required as an aid in designing new and better slot shapes. With such a numerical method it also ought to be possible to design such efficient slots that larger models could be allowed, yielding higher test Reynolds numbers. An even more challenging idea, of course, would be to provide old test sections with adaptable "smart" slots, as well as projecting coming generations of new facilities with such slots.

The main point in "numerical" tunnel runs should preferably be to establish and define the operating conditions of the real tunnel in order to minimize the difference between the tunnel run and the desired free-air reference flow in the neighborhood of the model. If corrections are needed they can be estimated by calculations.

Until now, theory has played a fairly minor role in the design of slot shapes. However, a couple of years ago Berndt[1] presented an inviscid theory of wall interference in slotted test sections. His theory resulted in a homogeneous wall boundary condition to be used for numerical calculations. Recently, Karlsson and Sedin[2] started some exploratory calculations applying Berndt's theory to axisymmetric test sections with uniformly distributed slots of constant width. The present paper is an extension of that investigation to incorporate slot shapes of varying width in the streamwise direction. Attempts are also made to design slot shapes inversely for which almost interference-free situations appear for a given axisymmetric body in the tunnel. This is carried out by imposing calculated free-air conditions in the homogeneous wall boundary condition from which a system of ordinary differential equations result, where one of the unknowns is the sought slot width. Berndt's theory also allows for effects of the plenum chamber pressure, the slot depth, and the number of slots, as well as their relative positions at the wall.

II. The Theory and Computational Procedures

The inviscid wall theory of Berndt[1] is built on the calculation of an approximate velocity perturbation potential $\bar{\varphi}$. In comparison with the "exact" solution φ, the approximate $\bar{\varphi}$ is created by averaging (filtering) φ with respect to higher order cross-flow variations caused by the slots and the walls in the test section. Utilizing slender-body cross-flow theory in combination with matched asymptotic expansions, the close details of the slot flow are coupled to the filtered potential through a pressure balance equation for each slot. This results in a homogeneous wall boundary condition for each slot giving a relation between $\bar{\varphi}$ and the radial velocity $\bar{\varphi}_r$ at the wall

$$\bar{\varphi}=\mathfrak{F}(\bar{\varphi}_r) \tag{1}$$

The functional $\mathfrak{F}$ in Eq. (1) includes the dependence on geometrical data such as the variable slot width $a(x)$, the slot depth l, and the number of slots N, as well as the normalized plenum chamber pressure δ. In a general three-dimensional case a trigonometric interpolation is needed between the slots to give a complete description of $\bar{\varphi}$ as a function of $\bar{\varphi}_r$ at the wall. Once the proper $\bar{\varphi}$ and $\bar{\varphi}_r$ are found it is possible to calculate the "exact" potential φ along the wall surface in order to evaluate the wall pressure. Close to the body $\bar{\varphi}$ is equivalent to φ. Equation (1) symbolizes the solution of three ordinary differential equations, which have to be solved simultaneously. One of the dependent variables in this system is the position of the line $y_p(x)$ (in the centerplane of each slot) where the plenum pressure is imposed.

III. Equations and Numerical Procedures

The basic field equation to be solved between the model and the tunnel wall is the axisymmetric small perturbation equation given by

$$(1-M_\infty^2-M_\infty^2(\gamma+1)\bar{\varphi}_x)\bar{\varphi}_{xx}+(r\bar{\varphi}_r)_r/r=0 \tag{2}$$

The potential $\bar{\varphi}$ is the filtered potential which is equal to or close to the "exact" solution φ in the neighborhood of the model. M_∞ is the freestream Mach number of the desired free-air reference flow, which the tunnel test is supposed to simulate as closely as possible around the model. Subsonic Mach numbers only are treated. In Refs. 3 and 4 a rapid finite-difference method was presented for solving transonic flow problems in cylindrical coordinates. This method decomposes the potential into two new functions F and G so that $F=r\bar{\varphi}_r$ and $G=\bar{\varphi}-\ell n(r)F$. These definitions, together with Eq. (2), will give the system

$$\begin{aligned} F_r &= -r(1-M_\infty^2-M_\infty^2(\gamma+1)\bar{\varphi}_x)(\ell n(r)F_{xx}+G_{xx}) \\ G_r &= r\ell n(r)(1-M_\infty^2-M_\infty^2(\gamma+1)\bar{\varphi}_x)(G_{xx}+\ell n(r)F_{xx}) \end{aligned} \tag{3}$$

Equations (3) are solved separately in an iterative manner, repeatedly going outward with F and inward with G. The values of $\bar{\varphi}_x$ in Eq. (3) are taken from the previous iteration. Initial values of F are given by the model geometry close to $r=0$ $(F=R(x)\mathrm{d}R(x)/\mathrm{d}x)$ and starting values of G are provided by solving Eq. (1) so that $G=\mathfrak{F}(F)$ at the chosen tunnel radius, $r=1$. The tunnel radius is the unit of length throughout this paper. The upstream inflow and downstream outflow conditions are given by $\bar{\varphi}_x=-\delta$ and $\bar{\varphi}_{xx}=0$, respectively. The chosen coupling of the inflow condition to the plenum pressure coefficient effectively sets the entrance Mach number M_0. This will be further commented upon in the next paragraph.

In the axisymmetric case, with a cylindrical test section $(r=1)$ provided with N equal and uniformly distributed slots of width $a(x)$, the wall condition [Eq. (1)] is equivalent to solving the following equations

$$q=2\pi\bar{\varphi}_r(x,1)/N \tag{4}$$

$$\mathrm{d}y_p/\mathrm{d}x=qv/a-\mathrm{d}A/\mathrm{d}xy_pE \tag{5}$$

$$\begin{aligned} &\mathrm{d}/\mathrm{d}x(\bar{\varphi}-\bar{\varphi}_0+qQ-q(\ell n(N)+A)/\pi-y_p^2\mathrm{d}A/\mathrm{d}xE/2) \\ &+(qv/a-\mathrm{d}A/\mathrm{d}xy_pE)^2/2+\delta=0 \end{aligned} \tag{6}$$

The variable q determined from Eq. (4) denotes the volume flux per unit length through each slot. $y_p(x)$, integrated through Eq. (5), is the line in the centerplane of the slot where the plenum pressure is specified in the mathematical model $(y_p>0$ inside slot). The symbol A is the natural logarithm of the slot width $(A=\ell n(a))$ and $E=E(y_p)$ is the unit step function equal to unity inside the slot. Equation (6) expresses the pressure balance along $y_p(x)$ and the approximation of the pressure contains a quadratic cross-flow velocity term. v and Q are the normalized velocity and velocity potential functions for an isolated slot of unit width and unit flux (see Ref. 1).

Equations (4-6) have to be solved simultaneously as the line $y_p(x)$ is not known a priori for given values of $\bar{\varphi}_r(x,1)$. This is done by a step-by-step integration technique starting at the beginning of the slot. The starting and the continuation of this integration process are not altogether trivial. This is due to the fact that a logarithmic singularity is at hand as $a\to 0$ and further that the flow entering the slot might split into two different streams, one leaving the slot penetrating into the plenum chamber as a thin jet and one that turns back and might flow into the test section again, carrying fast air with a bubble of quiescent plenum air on its back. Some remarks about this will be made in the next paragraph.

Now, summarizing Eqs. (2-6) the following computational scheme can be outlined in a direct mode calculation for given slot shape and tunnel conditions:

1) Guess a G and $\bar{\varphi}$ field, e.g., $G=\bar{\varphi}=0$.

2) Integrate the F equation [Eq. (3)] from the body to the wall. Initial values of F are given by the body geometry.

3) Evaluate the wall condition [Eq. (1)] through integration of Eqs. (4-6). This gives initial data for $G(G=\mathfrak{F}(F))$ at $r=1$.

4) Integrate the G equation [Eq. (3)] from the wall to the body.

5) Evaluate a new composed $\bar{\varphi}$ field $(\bar{\varphi}=\ell n(r)F+G)$. If the maximum correction in $\bar{\varphi}$ from the previous iteration to the present is greater than a specified convergence criterion, go back to step 2 and make a new run. Otherwise, terminate the calculations and evaluate the pressure distributions on the body and the wall surfaces.

In order to analyze the wall pressure, the filtered solution $\bar{\varphi}$ is matched to the complete "exact" solution φ in the neighborhood of the wall. According to Ref. 1 this will result in the following formula *halfway* between two neighboring slots.

$$\varphi=\bar{\varphi}(x,1)-\ell n(4)\bar{\varphi}_r(x,1)/N \tag{7}$$

The tunnel interference is in the present paper quantified by a single number called the figure of tunnel interference (FTI). It is based upon the difference in body surface pressure between the numerical tunnel run and the desired free-air case with the freestream reference Mach number M_∞. Thus the FTI is defined as

$$\mathrm{FTI}=\left(\sum_{i=1}^{n}(\Delta C_p)_i^2/n\right)^{1/2}\Big/|C_{p\min}| \tag{8}$$

$(\Delta C_p)_i$ is the pressure coefficient difference between the tunnel and the desired freestream case, the difference being evaluated at mesh point i. The symbol n denotes the number

of mesh points covering the body. $|C_{p\min}|$ is the absolute value of the minimum pressure on the body surface in the free-air reference case.

An inverse mode calculation designing an optimal slot shape for an almost interference-free flow about a given model is carried out as follows.

1) Calculate the desired free-air reference case with Mach number M_∞ for the actual model.

2) Assume the filtered solutions $\bar{\varphi}$ and $\bar{\varphi}_r$ to be equal to the free-air solutions and substitute $\bar{\varphi}(x,1)$ and $\bar{\varphi}_r(x,1)$ in Eqs. (4-6) by corresponding free-air values from step 1.

3) Assume some convenient values of the slot width a and its gradient da/dx at the beginning of the test section. Choose a slot depth l and a plenum pressure δ.

4) Integrate Eqs. (4-6) with respect to the slot width $a(x)$, advancing step by step toward the end of the test section. If the end is successfully reached with a physical slot shape, go to step 5. If not, go back to step 3 and change the parameters and go for a new run.

5) If necessary, make a smooth fairing of the found slot shape far upstream so that it starts with $a=0$. After this, perform a direct mode calculation to check the wall interference on the model.

An acceptable slot shape is usually found within one or two attempts.

IV. Numerical and Mathematical Models

Experimental investigations underlying the slot flow model of Ref. 1 showed that under typical test conditions the slot flow is not necessarily dominated by viscosity, and that therefore an inviscid flow model can be developed that is reasonably close to the physical reality. By using matched asymptotic expansions in combination with slender-body cross-flow theory it was possible to treat each slot separately in Ref. 1. The theory of Ref. 1 is based upon the assumption that the arc length between two neighboring slots is much larger than the width of a slot. The details of the slot flow model of Ref. 1 will not be repeated here, but some comments will be made in relation to the schematic slot flow situation as depicted in Fig. 1.

The upper part of Fig. 1 shows a cut through the centerplane of a slot. The lower part illustrates three different crossflow planes in regions I, II, and IV. Fast air from the test section enters the slot far upstream in region I and also in region II. As it turns out, due to the pressure field set up by the wind-tunnel model, the entering flow can be split up into two different streams, one penetrating the plenum chamber as a thin jet in region II and one fast stream coming back toward the test section in region III, completely leaving the slot in region IV with a bubble of quiescent plenum air on its back. In principle, this behavior can be repeated several times until the end of the test section is reached. At first sight, this type of slot flow really seems to be a bit complicated to describe in simple mathematical terms. However, Berndt[1] assumed an incompressible cross-flow velocity potential to exist in each plane, $x=$ constant, and described the separating free surface between the fast air and the quiescent plenum air by integrating the contact surface as a material surface while gradually moving the x plane downstream with the speed of the reference flow. The position of the free-plenum surface is required to apply the plenum pressure to the mathematical model. The cross-hatched line $y_p(x)$ in Fig. 1 lies on the free-plenum pressure surface in regions I, III, and IV. To simplify matters, the plenum pressure δ is imposed only along the line $y_p(x)$ in the slot centerplane. However in region II special considerations have to be taken and in this "jet region" the plenum pressure is applied along the cross-hatched line $y_p=y_{p0}(x)$ between the points A and B in Fig. 1, where the assumed plenum pressure isobar surface intersects the centerplane. Thus, in region II y_p is set to the value y_{p0} whenever y_p appears in Eq. (6) and in the right-hand side of Eq. (5). The flow reversal (splitting) takes place at point B in Fig. 1 and

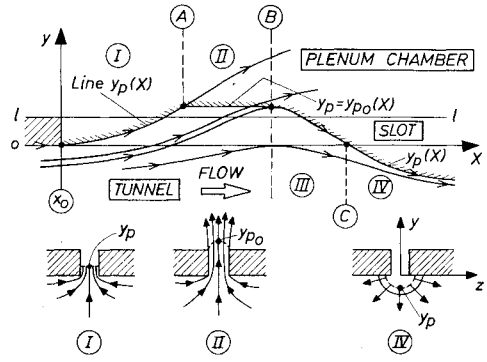

Fig. 1 Slot flow model.

this point is identified by $dy_p/dx=0$, which is checked via Eq. (5). The integration of y_p then continues into regions III and IV in very much the same way as in region I. Thus the complete line $y_p(x)$ is found tracing the plenum pressure isobar through the point stations x_0-A-B-C in Fig. 1.

The system equations (4-6) are successively integrated downstream step by step using a predictor-corrector type method. Special care has to be taken when starting this process at $x=x_0$, where the slot width is small or equal to zero. The slot flow functions Q, v, and y_{p0} can be found through the following equations

$$y_p/a=\left[-\sqrt{1+(s/\sigma)^2}-\ln\left(\left(\sqrt{1+(s/\sigma)^2}-1\right)/(s/\sigma)\right)\right]\sigma$$

$$\sigma=l/\pi \tag{9}$$

$$Q(0,y_p/a)=-\sigma\ln(s) \tag{10}$$

$$v(0,y_p/a)=1/\sqrt{1+(s/\sigma)^2} \tag{11}$$

$$y_{p0}/a=l/a+\ln(2)/\pi\left(1+2\exp\left(-2(\pi l/a+1)\right)\right) \tag{12}$$

In order to investigate, at least qualitatively, the influence of the tunnel wall boundary layer on the wall boundary condition, Eq. (4) is corrected with the slope of the boundary-layer displacement thickness δ^*, yielding the corrected slot flux

$$q=2\pi(\bar{\varphi}_r(x,1)+d\delta^*/dx)/N \tag{13}$$

Concerning the numerical calculation of the field between the wall and the wind-tunnel model, the situation is as depicted in Fig. 2.

In the calculations underlying the results of Ref. 2 it was found that the best numerical behavior far upstream was obtained when the entrance Mach number M_0 was matched to the plenum pressure, yielding the inflow condition $\bar{\varphi}_x=-\delta$. However, this was true only when the nose stagnation region of the body was far enough away so as not to disturb the inflow section. For large models inserted into relatively short test sections a more sophisticated inflow condition is needed to smoothly match the calculated field in the interior of the computational domain. Such theoretical models have been sketched but not yet extensively tested. However, this might not be a decisive problem (at least not for moderately sized models) as the plenum pressure and the slot shape at the model position seem to be dominant over minor changes in inflow data. At the outflow section the boundary condition is not so easily specified, which led to the neutral condition $\bar{\varphi}_{xx}=0$. The wall condition $G=\mathfrak{F}(F(x,1))$ or equivalently $\bar{\varphi}=\mathfrak{F}(\bar{\varphi}_r(x,1))$ is numerically applied by under-relaxing the correction obtained from one iteration to another to get a convergent procedure.

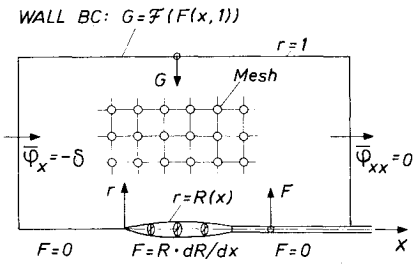

Fig. 2 Computational field model.

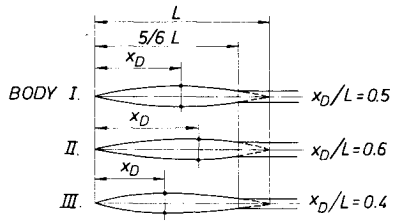

Fig. 3 Body geometries.

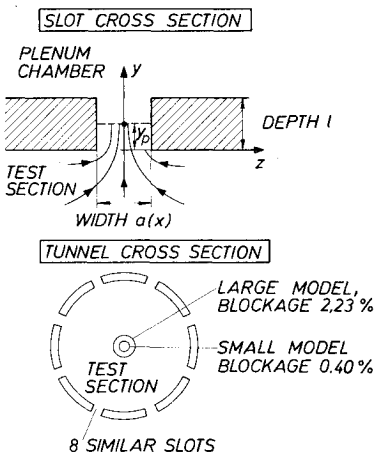

Fig. 4 Slot and tunnel cross sections.

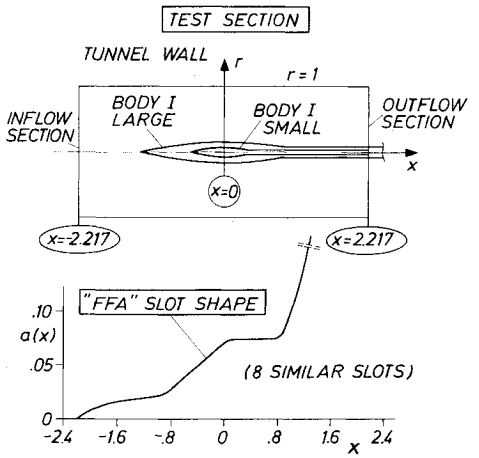

Fig. 5 Test section with nonoptimal FFA slot shape.

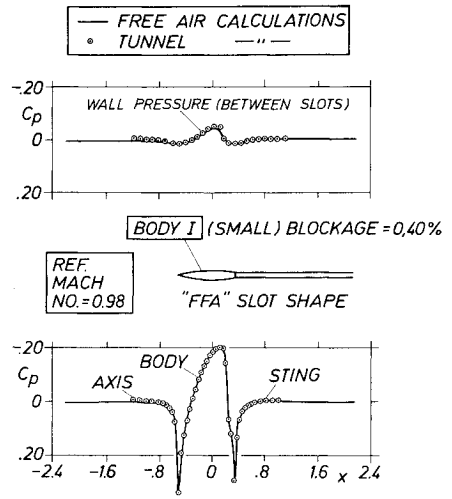

Fig. 6 Pressure distributions of body I (small) in tunnel with FFA slot at reference Mach number 0.98.

V. Body and Test Section Geometry Definitions

Three different bodies are considered in the calculations. The bodies are sketched in Fig. 3. The body shapes are characterized by a generalized parabolic arc defined by the equation

$$R(x)/L=\tau/2/(m-1)m^{m/(m-1)}(\xi-\xi^m) \quad \xi=x/L+1/2 \quad (14)$$

The symbol R denotes the body radius and τ is the ratio between the maximum diameter and the full theoretical length L.

The origin $x=0$, $r=0$ of the cylindrical coordinate system is placed in the middle of the distance L. The parameter m is used to alter the position of the maximum diameter, which is situated at a distance x_D from the nose tip. The bodies are truncated at a distance $5/6\,L$ from the nose point and the sting diameters follow from that. The slenderness parameter τ is equal to $1/(6\sqrt{2})$ in all cases. Body I is defined by $m=2$ and body II by $m=3.390$, while body III has $m=1.188$. The corresponding x_D/L values are 0.5, 0.6, and 0.4, respectively.

Figure 4 gives an impression of the tunnel cross section with a close view of the slot section including geometry definitions. The test section is provided with eight uniformly distributed slots and the tunnel wall is defined by $r=1$. The wall radius is here the unit of length in all applications. The largest body with a blockage ratio of 2.23% and the smallest body with one of 0.40% are shown in Fig. 4. These models have full lengths of $L=2.533$ and 1.078, respectively.

Figure 5 shows the dimensions of the test section considered and also the impressions of the largest and the smallest models of body I. The lower part of Fig. 5 gives the slot width distribution of a slot, which is called the "FFA" slot. This slot shape is close to the slot of an existing high-speed wind tunnel that is situated at the Aeronautical Research Institute of Sweden (FFA). The model size used in this tunnel does not usually exceed a blockage ratio of 0.5% and the model is then usually placed along x values corresponding to the constant value plateau of the slot width distribution. However, due to some practical scaling considerations the present calculations were performed by scaling the body sizes around $x=0$ as indicated in the upper part of Fig. 5. Thus, the model position is a bit ahead of that used in the real FFA tunnel. Moreover, to stress the wall interference theory, very large bodies are being computationally considered with blockage ratios of as much as 2.23%.

The constant value section of the FFA slot shape (Fig. 5) yields a total circumferential test section ventilation of about 9.44% in the numerical calculations.

To get a rough idea about the influence of a tunnel wall boundary layer on slot design, a turbulent flat-plate boundary layer was assumed in some exploratory calculations. In these investigations a Reynolds number of 5.4×10^6 m^{-1} was applied with an assumed boundary-layer thickness of 5 cm at $x=0$. The physical tunnel radius was then chosen to be 0.472 m which gives a test section area of 0.7 m^2. This area is the same as that of the real FFA tunnel.

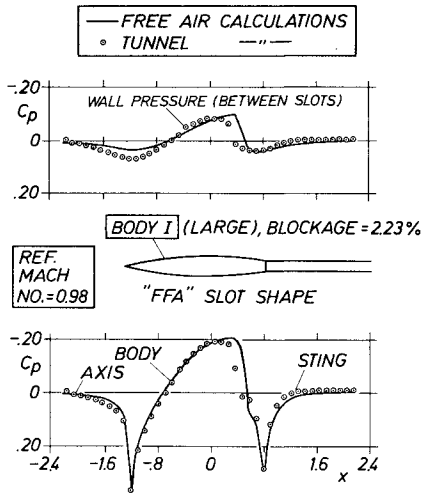

Fig. 7 Pressure distributions of body I (large) in tunnel with FFA slot at reference Mach number 0.98.

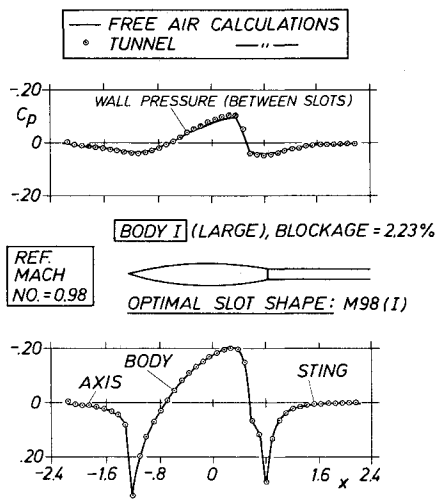

Fig. 8 Pressure distributions of body I (large) in tunnel with optimal slot M98(I) at $M_\infty = 0.98$.

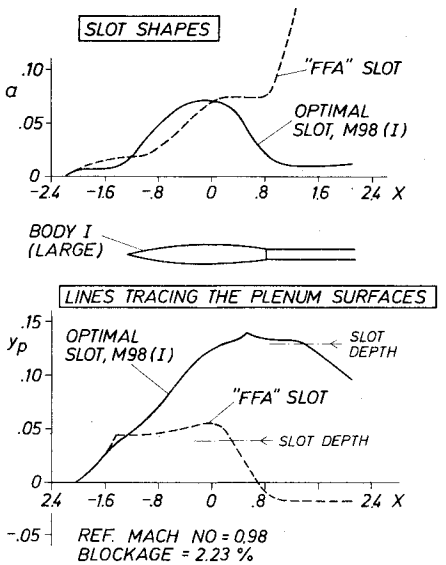

Fig. 9 Comparisons between optimal slot M98(I) and FFA slot.

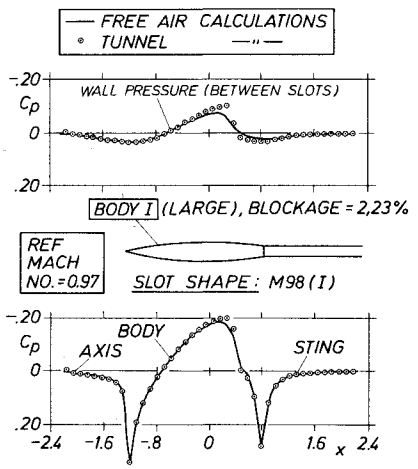

Fig. 10 Pressure distributions of body I with optimal slot M98(I) at off-design, Mach = 0.97.

VI. Calculated Results

Figures 6-17 show some numerical calculations and applications of the theory to wind-tunnel models of bodies I, II, and III of different sizes. The numerical study is primarily divided into four parts with different objectives.

The first part constituting Figs. 6 and 7 is to show the flow and interference situations for a moderately large model and a very large model in a test section with a conventional nonoptimal slot shape. The second part covering Figs. 8-11 has the objective of showing what can be done to the large interference of a big model by designing an optimal almost interference-free slot shape at a desired design Mach number. In this second part the situations at off-design Mach numbers are also demonstrated for the same body. The third part that is illustrated by Figs. 12-14 shows what happens when an optimally designed slot shape for one body is used together with other "off-design" bodies at the original design Mach number. The fourth part of the investigation considers Figs. 15-17 and is devoted to results from the inverse mode slot design procedure. In this part the design Mach number is varied for constant body geometry, whereupon the body geometry is varied for constant design Mach number. An investigation is also made to see how the optimal slot shape is affected by the blockage ratio with and without a tunnel wall boundary layer. No considerations concerning viscous boundary layers on the body surfaces have been made.

Table 1 gives some numerical data for the calculated cases shown in Figs. 6-17. Some of the slots are named according to the example M98(I), which means that the optimal design reference Mach number is 0.98 and the slot is designed for body I. Data are divided into five horizontal sections. Data missing in one section can be found in some of the previous sections.

The pressure distributions are calculated according to the formula

$$C_p = -2\varphi_x - \varphi_r^2 \tag{15}$$

A typical finite-difference mesh divides the test section into 60×40 points in the x and r directions, respectively. About 20 x points cover the body. A practical field convergence criterion is 10^{-6}-10^{-7} in the maximum potential correction, which usually is reached after about 150-200 iterations.

VII. Comments on the Numerical Results

Figure 6 shows a typical interference situation for a conventionally large model of body I ($B = 0.40\%$) at Mach $M_\infty = 0.98$. The model is calculated in the test section as shown in Fig. 5 with the nonoptimal FFA slot. As can be seen from the pressure distributions of the free-air case and the tunnel case the wall interference is rather low, a fact which is confirmed also by the FTI value of 0.007 found in Table 1.

Table 1 Data for calculated cases

Fig.	Body	B,%	M_∞	Slot	FTI	$-\delta$	l
6	I	0.40	0.98	FFA	0.007	0.0021	0.04
7	I	2.23	0.98	FFA	0.227	0.0021	0.04
8	I	2.23	0.98	M98(I)	0.011	0.0021	0.13
10	I	2.23	0.97	M98(I)	0.062	0.0021	0.13
11	I	2.23	0.99	M98(I)	0.099	0.0021	0.13
12	II	2.23	0.98	M98(I)	0.079	0.0021	0.13
13	III	2.23	0.98	M98(I)	0.154	0.0021	0.13
13	III	2.23	0.98	M98(III)	0.009	0.0021	0.13
15	I	2.23	0.97	M97(I)	–	0.0021	0.13
15	I	2.23	0.99	M99(I)	–	0.0021	0.24
16	II	2.23	0.98	M98(II)	–	0.0021	0.13
17	I	0.40	0.98	Optimal	–	0.0021	0.13
17	I	1.04	0.98	Optimal	–	0.0021	0.14

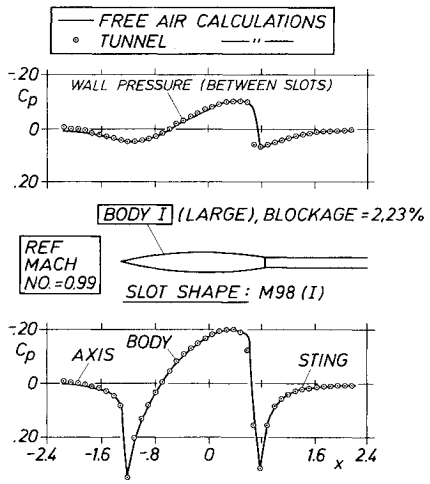

Fig. 11 Pressure distributions of body I with optimal slot M98(I) at off-design, Mach = 0.99.

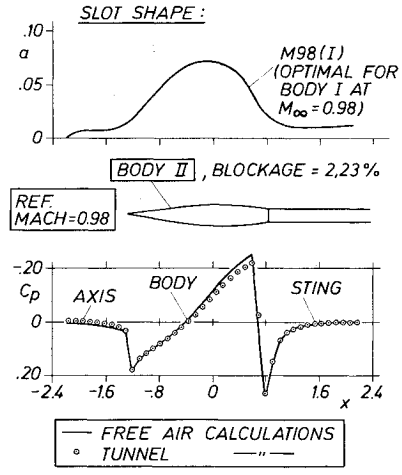

Fig. 12 Pressure distribution of body II in tunnel with slot M98(I) at reference Mach number 0.98.

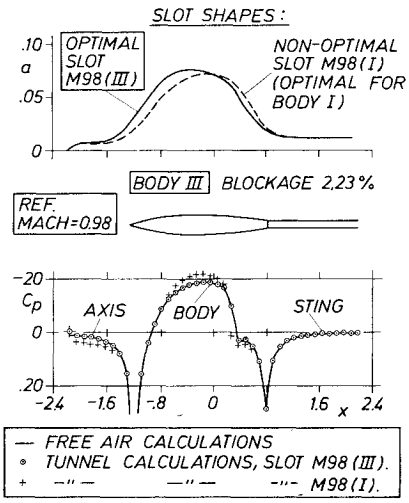

Fig. 13 Comparisons between pressure distributions of body III with optimal slot M98(III) and nonoptimal slot M98(I) at reference Mach number 0.98.

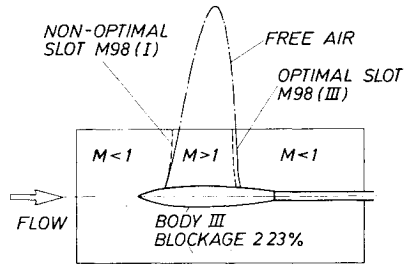

Fig. 14 Supersonic flow regions for body III in tunnel with slots M98(III) and M98(I) at reference Mach number 0.98.

However, if the model size is increased dramatically to give a blockage ratio of $B = 2.23\%$ (for the same body and test section) the situation will be as bad as depicted in Fig. 7. Compared to the previous case, the tunnel interference has now been increased from FTI = 0.007 to 0.227. To accept such a large model the level of interference must be diminished by at least one order of magnitude. One way to do that is to try to design a better slot shape by running the inverse mode design process as mentioned in Sec. III. If this is done and the same tunnel run is recalculated with the new slot shape, a much better interference situation appears as shown in Fig. 8. For this slot named M98(I) the agreement between the free-air reference distribution and that of the tunnel run is excellent on the body surface. The calculated pressures halfway between the slots are also in good agreement with each other. The FTI is now reduced to a moderate value of 0.011. The shape of the optimal slot M98(I) is found in Fig. 9 together with the conventional FFA slot.

In Fig. 9 the lines $(y_p(x))$ tracing the plenum surfaces are illustrated for the optimal M98(I) and the nonoptimal FFA

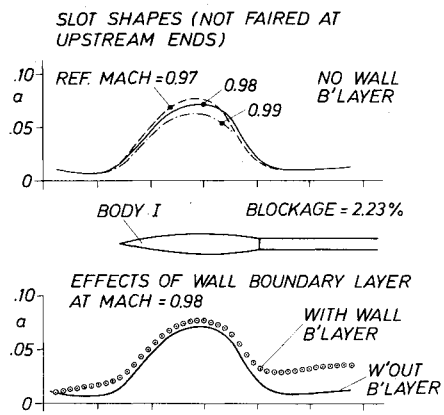

Fig. 15 Inverse mode designed slot shapes of body I at design Mach numbers 0.97, 0.98, and 0.99.

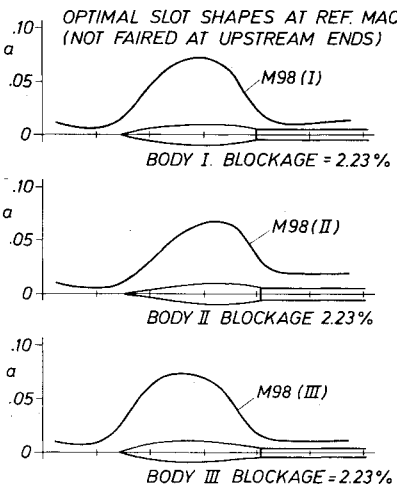

Fig. 16 Inverse mode designed slot shapes of bodies I, II, and III at design Mach number 0.98.

slot cases. It is here interesting to note that the FFA slot allows a bubble of quiescent plenum air to expand into the test section above the rear part of the body. However, the optimal slot is just filled up with fast air above the rear part of the body and flow entering the slot farther upstream does not have time to return with quiescent air on its back. This is a typical feature of an optimal slot having such a depth that no plenum air has time to enter the test section. The "jet regions" ($y_p = y_{p0}$) are reflected in the chopped off parts of the y_p lines slightly above the marked slot depths in Fig. 9. The normalized plenum pressures at y_p are the same in both cases (see Table 1).

One important observation to be made for the large model of Figs. 7 and 8 is that a slight discontinuity in the pressure gradients can be recognized at the inflow section, which is a symptom of the shortcomings of the assumed inflow boundary condition as shown in Fig. 2. This boundary condition is built on the assumption that the wind-tunnel model disturbs the inflow to a negligible degree only and that the asymptotic first-order behavior of $\bar{\varphi}_x$ close to the slot start can be estimated through Eq. (6) by introducing plausible power series expansions of y_p, a, and q. This simplified inflow model was shown to be adequate for moderately large wind-tunnel models up to a blockage ratio of about 1% as calculated in Ref. 2. However, to improve on the inflow situation for very large models a more sophisticated boundary condition is required.

In Figs. 10 and 11 body I ($B = 2.23\%$) is calculated with the optimal slot shape M98(I) at off-design Mach numbers 0.97 and 0.99, respectively. From Table 1 it can be seen that the

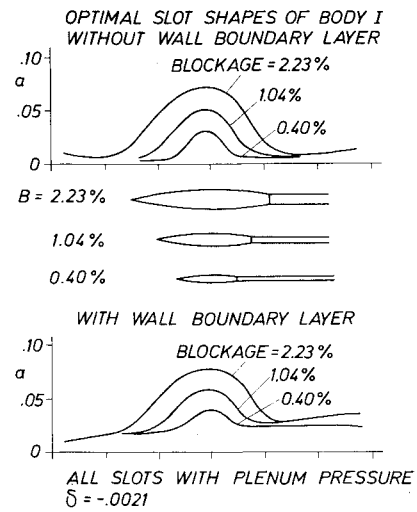

Fig. 17 Effects of tunnel blockage ratio on optimal design of slot shapes for body I at reference Mach number 0.98.

tunnel interference then is increased (from the "optimal" value FTI = 0.011) to FTI = 0.062 and 0.099, respectively. The differences between the desired free-air cases and the tunnel cases lie mainly in the shock-wave regions. An interesting feature is that the mentioned mismatch at the inflow section is less pronounced for the higher Mach number than for the lower, a fact which illustrates the difficulties for signals coming from the body to propagate upstream in flows with Mach numbers closer to unity.

Figures 12 and 13 show what happens when the slot M98(I), which is optimal for body I, is tested together with the off-design models (bodies II and III) at the original design reference Mach number 0.98. From Table 1 it follows that for these cases the tunnel interference is FTI = 0.079 for body II and FTI = 0.154 for body III to be compared to FTI = 0.011 at the original design point for body I. From Fig. 12 it can be seen that the inflow is smooth and well-behaved depending on the slender nose shape of body II. Body III, however, has a strong mismatch at the inflow section, which is illustrated in Fig. 13 by the cross symbols in the graph of the pressure distribution. This accentuated inflow mismatch depends, of course, on the not so slender forward part of body III. However, by running the slot design procedure for body III, the optimal slot shape M98(III) was designed as shown in Fig. 13. With this slot the interference was dramatically pressed down to FTI = 0.009 and the pressure distribution then agreed excellently with the free-air case at Mach 0.98, which also is illustrated in Fig. 13. The mismatch at the inflow section is diminished though still clearly visible for the optimal slot. Figure 14 shows the corresponding supersonic domains for body III.

Figures 15-17 show some pure inverse design mode calculations of optimal slot shapes with and without an assumed flat-plate turbulent wall boundary layer. The boundary-layer parameters are as defined at the end of Sec. V and the slot flux correction due to the displacement thickness is found in Eq. (13). As can be seen from Figs. 15-17 all slot width integrations are started with an initial value of $a = 0.01$, to be on the safe side against difficulties that might appear due to the logarithmic singularity of Eq. (6). For direct mode calculations a smooth fairing is made far upstream so that the slots start with $a = 0$.

Figure 15 shows the effects of the slot shape variations for different design Mach numbers ($M_\infty = 0.97$, 0.98, 0.99) for body I ($B = 2.23\%$). The maximum wall ventilation roughly ranges 8-10%, of which the highest value corresponds to the lowest Mach number ($M_\infty = 0.97$). The plenum pressure was kept constant but the slot depth had to be increased to carry through the integration for the highest Mach number

($M_\infty = 0.99$), see Table 1. The lower part of Fig. 15 gives the slot of body I with a wall boundary layer at $M_\infty = 0.98$. As can be seen from the graph, the slot has to be wider to compensate for the gradual thickening of the wall boundary layer. However, the total maximum wall ventilation increases only to about 9.8% (from about 9.2%), but far downstream the slot has to be opened a lot more.

Figure 16 shows variations in the optimal slot shape due to different body geometries without a wall boundary layer. The slot shapes have a close relationship with the geometries of bodies I, II, and III. There is, however, only a slight variation in the maximum slot width, the widest slot belonging to body III and the smallest to body II (which has the most slender nose).

Figure 17 shows the effects of the tunnel blockage ratio on the optimal design of slot shapes for body I. The blockage ratios considered are 0.40, 1.04, and 2.23%, respectively. The upper part of Fig. 17 gives the picture without a wall boundary layer while the lower part shows the situation with an assumed wall boundary layer. The plenum pressure coefficient is the same for all the slots and the slot depths are 0.13 or 0.14, see Table 1. It is interesting to note that the slot shapes with no wall boundary layer roughly seem to be scaled linearly with the square root of the blockage ratio. Moreover, the wall boundary layer affects the slot for the smallest model more than it does for the largest.

To conclude the inverse mode calculations, it should be pointed out that slightly different initial values at the beginning of a slot seem to alter the slot very little at the model position.

VIII. Conclusions

A numerical study has been made to investigate the consequences of an inviscid wall interference theory for slotted transonic test sections with respect to design and analysis of slot shapes. Encouraging results have been obtained and a simple procedure to design slot shapes that give almost zero interference on the body surface has been developed for reference Mach numbers of up to Mach 1. A great advantage of the present slot design procedure is that successful results can be obtained by using the desired free-air reference case as the only input. There is no need for repeated calculations of the nonlinear field about the wind-tunnel model to design the shape of a slot.

For moderately sized bodies the chosen coupling between the entrance Mach number and the plenum pressure seems to be working properly. However, for large wind-tunnel models in relatively short test sections the upstream disturbances from the body do not match the imposed inflow condition. In those cases a refined model of the inflow condition is needed. Thus far by experience, it has been found that the flow close to the body seems to be governed mainly by the plenum pressure and the slot shape right above the model, regardless of minor changes in the inflow. This is rather important when a reliable parameter strategy is to be established for the real tunnel.

References

[1] Berndt, S.B., "Inviscid Theory of Wall Interference in Slotted Test Sections," *AIAA Journal*, Vol. 15, Sept. 1977, pp. 1278-1287.

[2] Karlsson, K.R. and Sedin, Y.C.-J., "Axisymmetric Calculations of Transonic Wind Tunnel Interference in Slotted Test Sections," *AIAA Journal*, Vol. 17, Aug. 1979, pp. 917-919.

[3] Sedin, Y.C.-J., "Axisymmetric Sonic Flow Computed by a Numerical Method Applied to Slender Bodies," *AIAA Journal*, Vol. 13, April 1975, pp. 504-511.

[4] Karlsson, K.R. and Sedin, Y.C.-J., "The Method of Decomposition Applied in Transonic Flow Calculations," *Lecture Notes in Physics*, Vol. 59, Springer-Verlag, New York, 1976, pp. 262-267.